Variation of desolvation behaviour in two isostructural metal-organic frameworks based on a flexible, racemic bifunctional organic linker

Andrey A. Bezrukov, Karl W. Törnroos and Pascal D. C. Dietzel*[a]

Abstract: A racemic mixture of the chiral ligand 4,4'-(1,2-dihydroxyethane-1,2-diyl)dibenzoic acid was used to prepare two isostructural metal-organic frameworks, CPO-49-Zn and CPO-49-Mn, which contain coordinated solvent molecules at the metal site. The compounds showed different behavior upon desolvation. The dissociation of the solvent molecule from the metal site leads to single-crystal-to-single-crystal transformation. In CPO-49-Zn, a change of coordination geometry from trigonal bipyramidal to tetrahedral occurs at the zinc atom. In CPO-49-Mn, a rearrangement of coordination mode of a carboxylate group occurs instead, leading to a 4+1 coordination of the manganese cation in the form of a capped distorted tetrahedron. N_2 gas adsorption confirms that both desolvated structures are permanently porous. The behavior of the compounds upon heating has also been studied using variable temperature powder X-ray diffraction. The presence of a coordinated solvent molecule in the as-synthesized structures indicates the possibility to access the metal cation with reactive substrates. Both materials were evaluated in the catalytic oxidation of styrene. CPO-49-Mn showed significantly higher conversion than CPO-49-Zn material.

Introduction

Metal-Organic Frameworks (MOFs) are hybrid inorganic-organic crystalline materials where the inorganic part is represented by metal/metal cluster and organic part is the bridging polydentate linker.[1] Combining different inorganic and organic parts it is possible to obtain a variety of different structures with different properties for application in various areas, such as adsorption and catalysis.[2]

Synthesis of permanently porous MOFs with flexible linkers is often a challenge because the conformational freedom of the linkers might lead to structural rearrangement and loss of porosity when the guest molecules are removed from the pores. On the other side, the flexibility of the linker might result in new topologies and larger structural diversity than in case of a rigid bridging ligand.[3] Variable conformational angles around the metal node may also lead to flexible frameworks.[4]

Derivatives of ethane-1,2-diol with two adjacent hydroxy groups are attractive units to be incorporated into the MOF structure, because it might be used in a subsequent post-modification of the framework if the dihydroxy group does not participate in construction of the framework.[5] Previously, 1,2-di(4-pyridyl)glycol containing two 4-pyridyl groups connected to the glycol unit was successfully employed in syntheses of 2D[6] and 3D[7] networks. The pyridyl terminated linker has the disadvantage of being neutral (as long as the hydroxy groups remain protonated), which means either a charged framework is created or an additional anionic linker has to be present which takes the role of providing charge balance in the framework.

In the present work, we used 4,4'-(1,2-dihydroxy-1,2-ethanediyl)dibenzoic acid (H_4dhdba) (Scheme 1), which contains both a diol unit and terminal carboxylic acid groups. The hydroxy group carrying carbon atoms are asymmetric. Thus, an enantiomerically pure linker could be used to prepare homochiral MOFs.[8] Previously reported coordination polymer structures containing the H_4dhdba linker are either 1D or 2D coordination networks without permanent porosity.[9] Derivatives of the H_4dhdba linker, where two protons on hydroxy groups were substituted with a 1,1'-dimethylmethylene group[10] or two methyl groups[11], have also been used in the preparation of coordination networks.[10a, 11a, 11b, 10b, 11c] Herein, we successfully employed a racemic mixture of the H_4dhdba linker and Zn and Mn salts to build two isostructural 3D networks with permanent porosity, in which the dihydroxy group actually partakes in coordination of the metal. We also report the behavior of the new materials upon desolvation, heating and catalysis.

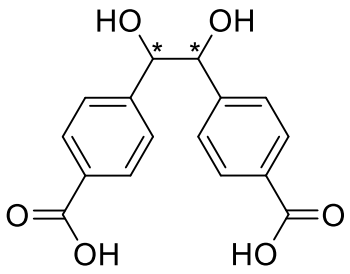

Scheme 1. 4,4'-(1,2-dihydroxyethane-1,2-diyl)dibenzoic acid (H_4dhdba).

Results and Discussion

The organic linker 4,4'-(1,2-dihydroxyethane-1,2-diyl)dibenzoic acid (H_4dhdba) was synthesized from the 4-formylbenzoic acid according to the literature procedure[12] (see Experimental details). The synthesis procedure applied by us

[a] Department of Chemistry
University of Bergen
P.O. Box 7803, N-5020 Bergen, Norway
E-mail: pascal.dietzel@uib.no
Internet: http://www.uib.no/en/persons/Pascal.Dietzel

Supporting information for this article is given via a link at the end of the document

yielded an equimolar mixture of (*S,S*)- and (*R,R*)-stereoisomers. In principle, the linker has a large degree of conformational freedom around the C(OH)–C(OH) bond. Originally, we selected the ligand with the aim to obtain porous coordination networks based on carboxylate metal bonds in which the hydroxy groups are still available for post-synthetic functionalization.[13a-c, 7c, 13d-f] However, the reaction conditions of the solvothermal synthesis, led to the formation of single crystalline products of composition $[M_2(Hdhdba)(HCO_2)DMF]\cdot DMF$ (CPO-49-M, M = Zn, Mn, DMF =N,*N*-dimethylformamide, CPO stands for Coordination Polymer of Oslo), which contain partially deprotonated diol groups and additional formate groups involved in coordination of metal cations and framework construction. Formate anions are sometimes encountered in MOFs as a result of hydrolysis of DMF during the solvothermal reaction.[14] The manganese and zinc compounds are isostructural to each other and an analogous cobalt compound.[15] To the best of our knowledge, it is the first MOF series in which the 1,2-dihydroxy groups of the H_4dhdba linker are partially deprotonated and participate in coordination of the metal cation in the framework. The crystal structure determination reveals that one of the guest DMF molecules is coordinated to a metal site, meaning there is a potential opportunity to obtain open-metal sites in the desolvated structure. The presence of coordinatively unsaturated metal sites frequently indicates broad potential for application of the material in adsorption and catalysis.[16]

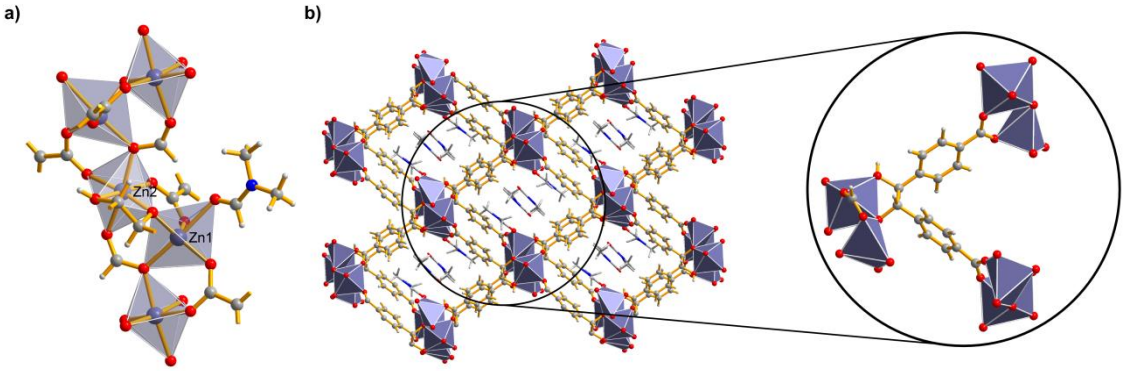

Figure 1. a) Secondary inorganic building unit in as-synthesized CPO-49-Zn (parallel to [010]; disorder in the C–C backbone is not shown for clarity), b) As-synthesized CPO-49-Zn framework structure, viewed along [010] (guest molecules in the pore are represented as sticks for clarity). As-synthesized CPO-49-Mn is isostructural.

Crystal structure of as-synthesized CPO-49-Zn and -Mn

The single crystal structure of CPO-49-Zn (Table S1) as obtained after synthesis (as-synthesized) contains two crystallographically independent Zn atoms in general positions. Zn1 is in a distorted trigonal bipyramidal coordination environment with τ = 0.80, where τ is an Addison parameter[17] indicating square pyramidal (τ = 0 for ideal), or trigonal bipyramidal (τ = 1 for ideal) geometry. Zn2 has octahedral coordination environment (Figure 1a). Zn2 is coordinated to both O atoms of the singly deprotonated diol group of one linker molecule and two oxygen atoms from two carboxylate groups of additional linker molecules in square planar fashion. The two perpendicular O atoms which complete the octahedral coordination environment belong to formate anions (Figure 1a). Zn1 is coordinated to the oxygen atom of the oxido group and two carboxylate oxygens in the equatorial positions. One axial position of Zn1 coordination environment is occupied by an oxygen atom belonging to a formate anion, while the second axial position is occupied by a DMF molecule coordinated through its oxygen atom. The octahedral and trigonal bipyramidal polyhedra are connected via common corners (corresponding to the oxygen atom of the oxido group of the partially deprotonated diol and the formate anion, respectively) and form infinite chains along the *b* axis. Each linker molecule interconnects three Zn chains: one chain by coordination with the oxido-hydroxy group and two chains by coordination with each of its carboxylate groups (Figure 1b). The coordination network can be described as rhombic arrangement with 1D chains of the inorganic secondary building unit in the corners and each organic linker participating in the formation of two wall sections. The 1D pore is filled with a second non-coordinating DMF molecule in addition to the DMF molecule coordinated to the metal site (Figure 1b).

The two oxygen atoms of the diol group are not equivalent to each other. One is protonated, while the second is deprotonated and bridges two adjacent Zn atoms. The difference in coordination and protonation is clearly reflected in the Zn–O distances. The Zn2–O2 distance of the protonated oxygen is 2.268(2) Å, while it is shorter for the deprotonated and consequently stronger coordinated O1 atom (d(Zn1–O1) = 1.9245(18) Å for and d(Zn2–O1) = 2.0096(18) Å, see also Table S2).

As-synthesized CPO-49-Mn is isostructural to as-synthesized CPO-49-Zn with analogous coordination

environments of the two crystallographically independent Mn atoms (trigonal bipyramidal for Mn1, with τ = 0.86, and octahedral for Mn2). Selected metal-oxygen distances and oxygen-metal-oxygen angles for Mn and Zn structures are listed in Table S2.

We used an equimolar mixture of (*R,R*)- and (*S,S*)-stereoisomers in the synthesis. There have been cases in which a chiral coordination network was spontaneously resolved from the racemic mixture of linkers [18] or even using achiral linkers.[19] However, we did not observe spontaneous resolution, i.e. the formation of crystals of opposite chirality in which the diastereomers are separated. Instead, the stereoisomers are built into the framework in equimolar amounts. The asymmetric unit contains a $Hdhdba^{3-}$ anion, in which the asymmetric C atoms of the ethane backbone and the hydrogen atom bonded to them are disordered, meaning that there is a mixture of (*S,S*)- and (*R,R*)-diastereomers on the position in the crystal structure. Because the corresponding oxidohydroxy groups of both stereoisomers are not disordered themselves, they are able to coordinate the metal with the α-oxidohydroxy group without distortion of the overall framework structure. Thus, in principle, it should be possible to synthesize the analogous homochiral porous structure using the pure enantiomer of the organic linker.

Crystal structure of desolvated CPO-49-Zn and -Mn

A gentle procedure of removing the solvent from the as-synthesized single crystals was performed by soaking the sample several times in chloroform to replace the high boiling DMF with a more volatile solvent. Afterwards, the chloroform was removed by heating the samples in a dynamic vacuum at 90 °C overnight. Both samples remained single crystalline, indicating that the solvent removal proceeded in form of a single-crystal-to-single-crystal transformation.[20]

The single crystal structure determination confirms that both compounds are permanently porous. No solvent was located in the pores as reflected by the absence of significant electron density in the pore space. Both, desolvated CPO-49-Zn and -Mn, still contain one-dimensional inorganic secondary building units composed of condensed coordination polyhedra around the metal cations which are connected by the organic linkers into the framework. However, despite the fact that as-synthesized CPO-49-Zn and -Mn are isostructural, the coordination environment of the metal cations with coordinated solvent rearranges differently for the zinc and manganese compounds. In CPO-49-Zn, the removal of the coordinated solvent molecule carrying atom O9 causes a decrease of coordination number of Zn1 from 5 to 4 and change of coordination geometry from trigonal bipyramidal to tetrahedral (Figure 2a-b) with Zn–O distances in the range 1.913(2)-2.009(2) Å and O–Zn–O angles in the range 102.20(10)-122.98(10)° (Table S2). The largest absolute change in distance is observed for the Zn1–O7 distance which decreases from 2.100(2) Å to 2.009(2) Å in the as-synthesized and desolvated structure, respectively. In contrast, the Mn1 atom retains the coordination number 5 after the loss of coordinated DMF molecule. This is a result of a change in coordination mode by one of the carboxylate groups. In the as-synthesized form, it coordinates Mn1 and Mn2 with each one of its oxygen atoms, while it rearranges in the desolvated form so that one oxygen atom coordinates both Mn1 and Mn2 (Figure 2c, d). The O9 atom belonging to DMF leaves the coordination environment while O3 from the carboxylate enters the coordination environment of Mn1, which is demonstrated by the change of the Mn1–O3 distance from 3.4853(23) Å in the as-synthesized to 2.364(2) Å in the desolvated structure. The coordination geometry of Mn1 changes from trigonal bipyramidal (τ = 0.86) to a shape best described as severely distorted square pyramidal (τ = 0.09) or capped distorted tetrahedron with four Mn–O distances in the range 1.9988(18)-2.1565(18) Å and one with 2.364(2) Å and O–Mn–O angles in the range 57.84(7)-138.48(7)°. Another effect of the rearrangement of the carboxylate coordination mode is that the connection of the Mn coordination polyhedra changes from corner-connected to edge-connected. This is reflected in larger changes of metal-metal distances (M1–M2) for the Mn compound than the Zn compound as it changes from as-synthesized to desolvated structure (Table S2).

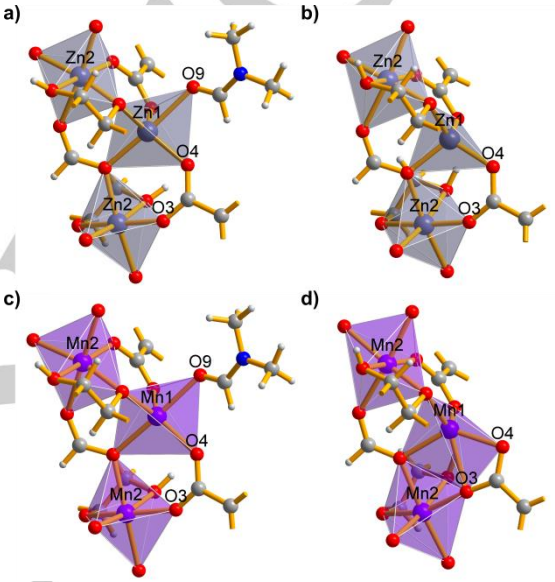

Figure 2. Coordination environment of the two crystallographically unique transition metal atoms in a) as-synthesized CPO-49-Zn, b) desolvated CPO-49-Zn, c) as-synthesized CPO-49-Mn, d) desolvated CPO-49-Mn. The corresponding bond lengths are listed in Table S2. Anisotropic thermal displacement ellipsoids are drawn at 50% probability. Extended structure surrounding of the polyhedra is represented in the in Figures S1-S2.

Atoms Zn2 and Mn2 are not coordinated by a solvent molecule. All the coordinating groups are contributed by 4,4'-(1,2-oxidohydroxidoethane-1,2-diyl)dibenzoate and formate ligands. The octahedral coordination environment of Zn2 and Mn2 remains essentially unchanged in the desolvated compound.

In congruence to the changes in the chain, the conformation of the flexible linker rearranges during the desolvation process. The torsion angle between the C–C bonds changes for both structures (Table S2).

The conformational flexibility of the organic linker and the rigidity of the framework structure influence the ease of change in coordination environment of the metal cation. Removal of coordinated solvent in rigid frameworks leads to the presence of coordinatively unsaturated metal sites (open metal sites), for example, as observed for the CPO-27 series.[21] In the case of CPO-49-Zn, the removal of the solvent molecule from Zn1

results in a change of coordination environment from trigonal bipyramidal to tetrahedral. An analogous rearrangement in a MOF has been observed for $[Zn_3(ntb)_2(EtOH)_2]_n \cdot 4n$EtOH [22], in which a reversible single-crystal-to-single-crystal transformation upon loss of coordinated ethanol. Additional examples of single-crystal-to-single-crystal transformations with Zn containing MOFs induced by the loss of coordinated solvent molecule include the transformation from non-interpenetrated to interpenetrated structure in $[Zn_7O_2(nbd)_5(DMF)_2]$,[23] while exchange of coordinated solvent led to a change of topology for $[Zn_2(mtc)(DMF)_4]\cdot 2DMF\cdot 4H_2O$, in which complete exchange of DMF by soaking crystals in CH_2Cl_2 resulted in a unique 2D to 3D structural transformation that increased the porosity and sorption capacity.[24]

In CPO-49-Mn like in CPO-49-Zn, desolvation does not lead to the formation of an open metal site. However, instead of a straightforward change in coordination geometry as observed for the Zn1 atom, a change of carboxylate coordination mode is observed which leads to the 4+1 coordination of the Mn1 atom and the change in connectivity in the 1D inorganic secondary building unit. To the best of our knowledge, this is the first time such a single-crystal-to-single-crystal structural transformation has been observed for a manganese MOF. There are significantly fewer manganese MOFs reported in the literature than Zn MOFs and, consequently, fewer examples of single-crystal-to-single-crystal transformations induced by the loss of the solvent on the Mn^{2+} ions. One of the few examples of single-crystal-to-single-crystal transformations of manganese-organic frameworks is the hydration induced transformation of 2D $[Mn_3(ip)_3(bipy)_2]\cdot 2H_2O$ to 1D $[Mn(ip)(bipy)(H_2O)_2]\cdot H_2O$.[25]

The simultaneous flexibility of the chain and linker results in different rearrangements for the Zn and Mn structures. The difference between Zn1 and Mn1 behavior can be rationalized with the difference in ionic radii. The Mn^{2+} ion is larger than Zn^{2+}, and it prefers a higher coordination number.

Sorption experiments

Nitrogen sorption confirms the permanence of porosity indicated by the single crystal structures of the desolvated compounds. Both materials display reversible sorption isotherms (Figure 3), as expected for microporous materials. However, the shape deviates from an ideal type I isotherm, particularly for CPO-49-Mn, in that several steps occur above a nitrogen uptake of 130-150 cm^3 (STP) g^{-1}. Such steps are frequently related to changes of the structure of the adsorbant at the corresponding pressure. For example, steps occur in the MIL-53-type MOFs due to the gate opening effect.[26] Based on the flexibility of the ligand and the contraction observed on transition from the solvated to desolvated crystal structure (~3% and 7% for CPO-49-Zn and -Mn, respectively), it is reasonable to assign the occurrence of the steps to the response of the framework structure to increasing amounts of adsorbate in the pores. Application of the Langmuir equation to the lower pressure region yields specific surface areas of 853 m^2 g^{-1} for CPO-49-Zn and 647 m^2 g^{-1} for CPO-49-Mn, respectively. The BET specific surface area is 730 and 578 m^2 g^{-1} for CPO-49-Zn and -Mn, respectively. The observed pore volume (at p/p_0 = 0.5) is 0.30 cm^3 g^{-1} for CPO-49-Zn and 0.25 cm^3 g^{-1} for CPO-49-Mn, which corresponds well with calculated values based on the single crystal structures (see ESI, Table S3).

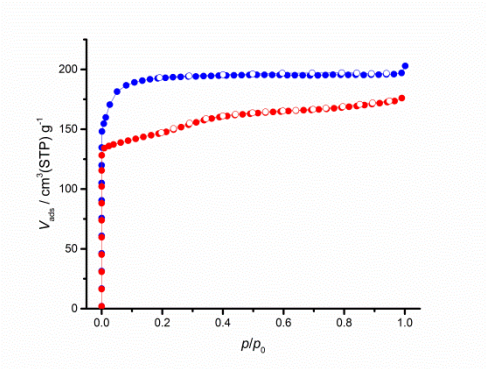

Figure 3. Nitrogen adsorption (full) and desorption (empty) isotherms on CPO-49-Zn (blue) and CPO-49-Mn (red) at -196 °C.

The desolvation of the CPO-49-M frameworks is a reversible process, as it was shown by the resolvation of the desolvated material. The powder X-ray diffraction patterns of bulk material after adsorption resolvated with DMF are similar to the patterns of as-synthesized material for both CPO-49-Zn and –Mn (Figures S7 and S8).

Thermal analysis

Thermogravimetric analysis indicates that the CPO-49-M materials undergo two processes during the heating: loss of the solvent (coordinated to metal sites and/or distributed in the pores) and decomposition of the framework.

For CPO-49-Zn in both O_2/Ar (20/80) and Ar atmosphere (Figure 4), the first mass decrease occurs in the range 32-300 °C that corresponds to loss of solvent. The second mass decrease is observed at ~440 °C and is typical for the decomposition of the material. The two processes of solvent loss and decomposition occur at widely spaced temperatures, in between which a plateau at ~78 mass-% is observed. However, a small exothermic peak at ~250 °C in the DSC signal in O_2/Ar may indicate that the desolvated framework starts to undergo further changes at lower temperature than implied by the mass loss and intense exothermic peak at ~440 °C that accompany the ultimate decomposition of the material and formation of crystalline ZnO (Figure S9).

In the case of CPO-49-Mn, solvent loss and decomposition of the framework appear to occur at more similar temperatures. As a consequence, no plateau is observed in the TG trace. Instead, it shows only a gradual decrease of mass without well resolved steps until final exothermic combustion. Again, a less intense exothermic peak occurs at ~180 °C in O_2/Ar (20/80). The ultimate mass loss occurs after 400 °C with a significantly more intense exothermic peak in the DSC signal than in case of the Zn material, fitting well to the observation that the inorganic residue is Mn_2O_3 (Figure S10), i.e. an additional redox process takes place in the form of oxidation of Mn^{2+} to Mn^{3+}. While the final decomposition step occurs at almost the same temperature for the zinc compound in argon and oxygen/argon mixture atmospheres, this step occurs at slightly higher temperature in argon than in oxygen/argon mixture for the manganese compound.

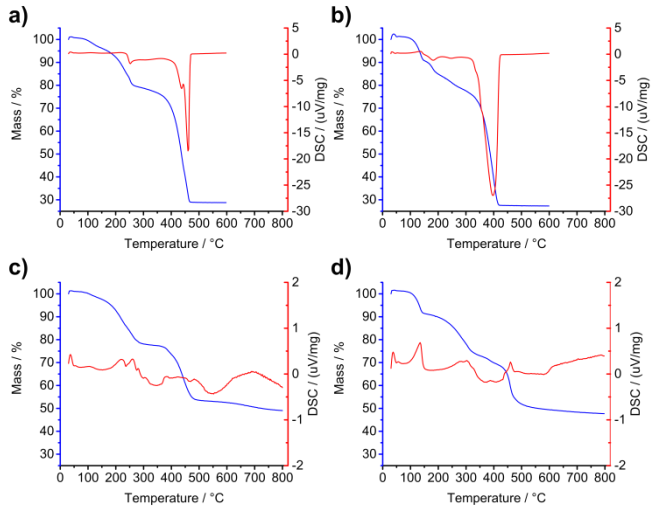

Figure 4. Simultaneous thermogravimetric analysis (blue) and differential scanning calorimetry (red) of a) CPO-49-Zn in O_2/Ar (20/80), b) CPO-49-Mn in O_2/Ar (20/80), c) CPO-49-Zn in Ar, d) CPO-49-Mn in Ar.

Variable temperature powder X-ray diffraction

Powder X-ray diffraction under operation conditions is a powerful technique to obtain additional information about how a crystalline metal-organic framework reacts to external stimuli.[27] Thermogravimetric analysis gives information only about the mass change, but it does not provide any information about changes in crystal structure of the material during heating. Variable temperature powder X-Ray diffraction in inert gas flow provides this complementary information.

In the case of CPO-49-Zn, the powder diffraction patterns before and after flow through the sample cell commenced look almost identical (Figure S13 and S14). A phase that is derived from as-synthesized CPO-49-Zn exists in the temperature interval from room temperature to ~150 °C. We observe a smooth change of lattice parameters for this phase up to ~100 °C (Figure 6). From ~100 °C upwards, a second phase starts to manifest while the first phase disappears. This discontinuous phase transition happens in the temperature range ~100-150 °C. The second phase has additional reflections at 2Θ = ~2.1 and ~3.2°, i.e. at lower angles than the first reflection of the room temperature phase. This would be in accordance with a decrease of symmetry of the structure or the increase in volume of the unit cell. Despite the fact that the second phase has one very intense reflection, there are only few reflections at higher angle which are well resolved. With the quality of the data available, attempts to index this phase were unsuccessful. Although thermogravimetric data showed ultimate mass loss for CPO-49-Zn after 450 °C, it was found that Zn sample has lost all crystallinity at about 350 °C (Figure 5). In fact, the intensities of the reflections in the powder pattern degrade visibly above ~240 °C (Figure S11), in tune with the exothermic peak observed in the DSC measurement.

We would like to point out that the second phase does not correspond to the single crystal structure of desolvated CPO-49-Zn (Figure S15). The simulated powder pattern from the desolvated single crystal CPO-49-Zn actually looks very similar to the powder pattern of solvated as-synthesized CPO-49-Zn. We ascribe this to the use of the gentle desolvation procedure (described above) which led to complete removal of the solvent from the pores at 90 °C, which is below the temperature where the phase transition starts to happen. The desolvated single crystals and the bulk material used in the adsorption experiments were treated in this way.

The main difference between the powder patterns of as-synthesized and desolvated CPO-49-Zn is the relative intensity of the [002] reflection. It seems to be characteristic for the amount of solvent present in the structure. While it is almost as intense as the reflection with maximum intensity in the powder pattern of solvated structure, it has dropped to approximately 1/3 of its intensity in the powder pattern of the desolvated structure (Figures 5 and S16). This decrease in intensity gradually occurs in the temperature range from 25 °C to 100 °C concomitantly with the decrease of the framework solvation in that temperature interval. However, at 100 °C not all molecules of the high-boiling DMF have been removed in the variable temperature powder X-ray diffraction experiment, meaning that the intensity of the [002] reflection did not decrease to quite as low levels as expected from simulated powder pattern of the single crystal structure determination.

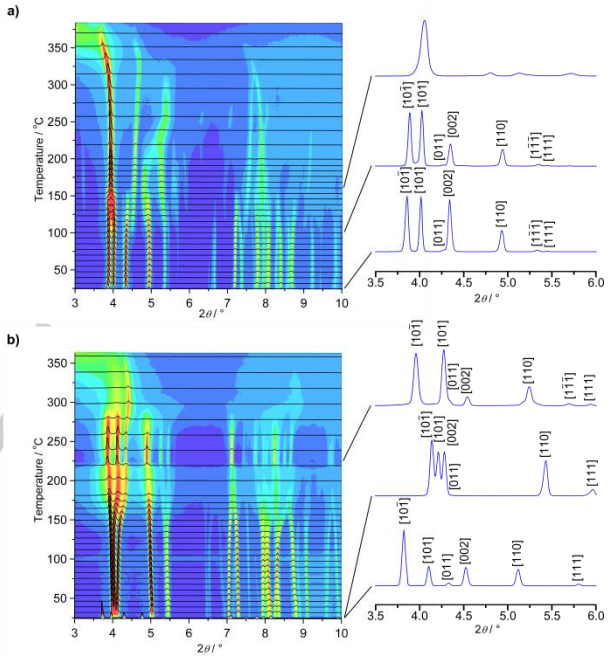

Figure 5. 2D variable temperature powder X-ray diffraction plot of a) CPO-49-Zn in Ar flow, b) CPO-49-Mn in He flow. Note the significant change in patterns of CPO-49-Mn before and after the gas flow through the capillary was switched on (the first pattern of CPO-49-Mn on the bottom was measured without flow). Representative powder X-ray diffraction patterns with reflection labels are shown on the right. At 220 °C, radiation damage was observed for the Mn sample and the sample was moved 0.5 mm upstream and perpendicular to the beam which lead to a significantly improved pattern, but also introduced a discontinuity in evolution of the patterns between the corresponding scans.

The as-synthesized sample of CPO-49-Mn, installed in the variable temperature setup but before the inert gas flow was switched on, corresponds well with the theoretical powder pattern calculated from the single crystal structure determination (Figure S18 and S19). The first pattern collected after the gas flow was switched on already shows dramatic shifts in reflection positions, reflecting significant changes in lattice parameters.

Apparently, the cell volume decreases by ~6% already upon commencement of the desolvation process (Figure S20). After this first sharp change, the diffraction patterns change more smoothly in the temperature range from room temperature to 220 °C, in congruence with continuous changes of the lattice parameters (Figure 6). Unfortunately, we observed radiation damage of the sample at 220 °C, as indicated by the decrease of intensity and change of the color of the sample in the beam. For that reason the sample was moved 0.5 mm upstream which led to a significantly improved pattern. Although this operation resulted in a small discontinuity of the evolution of pattern and lattice parameters, the change of lattice parameters follow the previous trend. The high temperature phase corresponds well to the empty one from the desolvated single crystal structure CPO-49-Mn-desolvated (see Figure S21 and S22). The Mn sample has completely lost its crystallinity at approximately 300 °C (Figure 5).

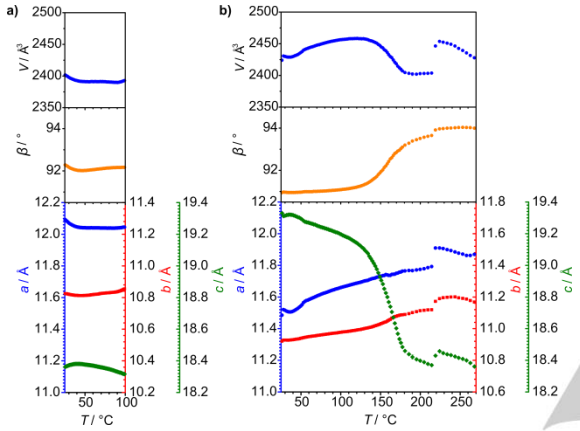

Figure 6. Evolution of lattice parameters with temperature for a) CPO-49-Zn (only up to 100 °C; there is no data available for the second crystalline, but non-indexed phase appearing at temperatures above 100 °C), b) CPO-49-Mn (for the full temperature range in which a crystalline phase was observed).

Catalysis

Oxidation of double bonds is an important reaction in organic chemistry. Enantioselective epoxidation[28] is especially of interest, because chiral epoxides can be transformed into other chiral molecules.[29] The CPO-49-M materials are good candidates for catalysis because of potentially accessible coordination site at the cation. CPO-49-Zn and -Mn discussed here contain a racemic mixture of the linker, and therefore cannot be used as the catalysts in enantioselective reactions. However, if one wished to do so the homochiral coordination polymer with the chiral linker could be synthesized in all likelihood, as discussed above. Here, we limited ourselves to test the potential catalytic activity of CPO-49-M using the oxidation of styrene (as model molecule bearing a C=C double bond) with *tert*-butyl hydroperoxide.

While CPO-49-Zn showed only limited conversion, CPO-49-Mn showed high conversion after a few hours (Figure 7). This result corresponds well with a previous study, in which styrene oxidation was catalyzed by the open metal site frameworks CPO-27-M (M-MOF-74), and where the CPO-27-Mn framework showed the highest conversion, while the CPO-27-Zn framework showed the lowest conversion among the -Mn, -Mg, -Ni, -Zn, -Co frameworks.[30]

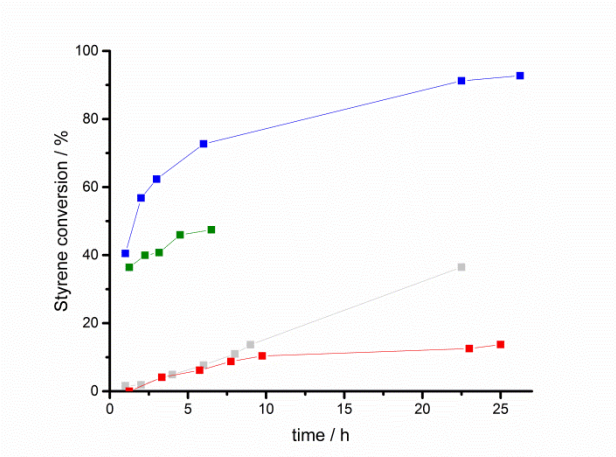

Figure 7. Kinetics curves for catalytic experiments of oxidation of styrene with *tert*-butyl hydroperoxide with CPO-49-Zn as the catalyst (red), CPO-49-Mn as the catalyst (blue), blank experiment without the catalyst (grey) and leaching test (green, CPO-49-Mn catalyst was centrifuged off after 1 h).

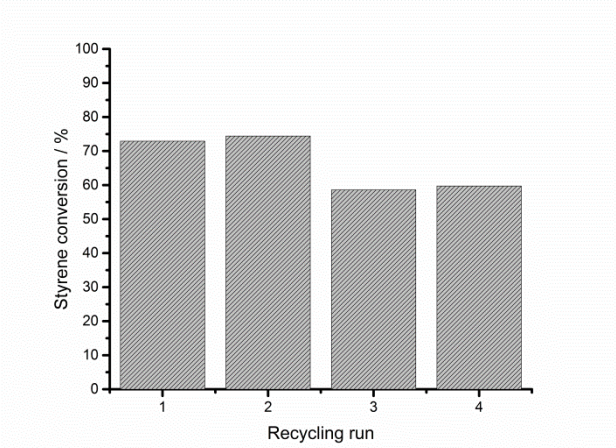

Figure 8. Recycling of the CPO-49-Mn in styrene oxidation reaction. Reaction time is 10h.

After the catalytic reaction run, the powder diffraction pattern of CPO-49-Zn remained more resolved than that of CPO-49-Mn (Figure S23), i.e. while the zinc compound was less reactive in the catalytic test, its long range structure was also less affected by the oxidative environment. The loss of long range structure of CPO-49-Mn was accompanied with a significant loss of specific surface area (Figure S24). The pore volume decreased by approximately 80%. ICP analysis of the supernatant solution indicates that there is no leaching of Mn^{2+} ions into the solution which means the catalytic activity is of heterogeneous nature.

CPO-49-Mn was also tested for reusability. After 10 hours catalytic reaction the solid was separated by centrifugation and used in a new catalytic run. The catalyst still showed significant conversion of styrene, although a drop of conversion from ~73% to ~59% is observed between runs 2 and 3 (Figure 8), probably due to mechanical loss of the catalyst. A leaching test was also performed for CPO-49-Mn (Figure 7). After initial conversion after 1 h reaction, CPO-49-Mn was centrifuged off from the

reaction mixture and the conversion of styrene in supernatant was monitored over the time. An increase of conversion over time is still observed after the removal of the solid catalyst. This is likely due to thermal conversion: the slope of styrene conversion after removal of the solid catalyst is comparable with the slope of the blank experiment.

Based on the experimental results above, we concluded that the catalytic reaction is of heterogeneous nature. The catalytic activity of CPO-49-Mn persisted despite a large loss of its structural order and surface area, indicating that the active sites on the outer surface of the material are possibly involved in the conversion of substrates. The material is reusable and shows activity in at least 4 catalytic runs of styrene oxidation.

Conclusions

We have managed to build two new isostructural frameworks using Zn^{2+} and Mn^{2+} cations and a flexible bifunctional linker. It is the first MOF series, where hydroxy groups of this linker are involved in coordination to the metal, leading to permanently porous frameworks with 1D channels.

The high crystallinity and crystal size of the materials allowed to follow the single-crystal-to-single-crystal transformations in the material upon removal of DMF solvent molecules coordinated to the metal site and from the pore. Both isostructural frameworks undergo a rearrangement of coordination environment and circumvent the formation of an open metal site. In case of the manganese compound, a rearrangement of the carboxylate group takes place leading to a 4+1 coordination environment.

Even though the racemic mixture of the linker was used in the synthesis, the structure allows one to anticipate that a homochiral MOF could be built from the enantiomerically pure linker. The presence of a solvent accessible metal site means the material could potentially be evaluated in asymmetric catalysis. In initial catalytic tests, the Mn compound showed higher conversion than the Zn compound.

Another promising way of the development of this MOF series is to elongate the linker molecule by increasing the number of phenyl rings in order to obtain larger pores.[10b, 11c] That potentially will greatly affect the pore size and consequently will lead to higher surface area and better pore accessibility.

Experimental Section

Materials

All chemicals, reagents and solvents were purchased from Sigma Aldrich and used as received without further purification, if it is not stated specifically. Hexane, toluene, THF and CH_2Cl_2 for inert syntheses were dried using Solvent Purification System (MBraun SPS-800). Manipulations under inert atmosphere were performed either in glove box (MBraun) or using Schlenk line technique. The gases were purchased from Yara Praxair and were of 99.999% purity or higher.

Crystallography

Suitable crystals for diffraction experiments were mounted in a minimum amount of Parabar 10312 oil (Hampton Research) in a nylon loop. As-synthesized single crystals were mounted at ambient conditions. Desolvated single crystals were mounted in the glove-box and transferred into the cryostream in a sealed shuttle. Intensity data was collected with a Bruker AXS TXS rotating anode system with an APEXII Pt^{135} CCD detector using graphite-monochromated Mo Kα radiation (λ = 0.710 73 Å). Data collection and data processing were done using APEX2,[31] SAINT,[32] and SADABS[33] version 2008/1, whereas structure solution and final model refinement were performed using SHELXS[34] version 2013/1 or SHELXT[35] version 2014/4 and SHELXL[36] version 2014/7.

CCDC 1483106-1483109 contain contains the supplementary crystallographic data for this paper. These data can be obtained free of charge from The Cambridge Crystallographic Data Centre via www.ccdc.cam.ac.uk/data_request/cif.

Synthetic procedures

[$TiCl_3$·3THF]. [$TiCl_3$·3THF] was synthesized according the literature procedure.[37] In a glove box, $(TiCl_3)_3$·$AlCl_3$ (20 g, 0.0335 mol) was suspended in toluene (20mL) in a Schlenk flask. The flask was subsequently transferred to a fume hood and operated using standard Schlenk techniques under Ar. The reaction mixture was cooled down to -50 °C and dry THF (150 mL, 1.8 mol) was added via cannula transfer. The purple suspension was then heated for 14 hours under reflux. The green reaction mixture was allowed to cool to room temperature and filtered under Ar atmosphere. The product was washed with dry hexane and dried in vacuo. The resulting blue powder (yield: 34 g, 94%) was stored under Ar at 2-8 °C.

H_4dhdba linker. 4,4'-(1,2-Dihydroxyethane-1,2-diyl)dibenzoic acid was synthesized based on a slightly modified literature procedure.[12] [$TiCl_3$·3THF] (34.0 g, 91.7 mmol) were dissolved in dry CH_2Cl_2 (50 mL) under Ar in a flask. In another flask, 4-formylbenzoic acid (13.7 g, 91.3 mmol) were suspended in dry CH_2Cl_2 (100 mL) under Ar. The titanium chloride complex solution was added to 4-formylbenzoic acid suspension via cannula transfer. The reaction mixture was stirred for 2.5 hours under inert conditions at room temperature. Then, water (150 ml) was added to quench the reaction. The resulting white precipitate was filtered and washed with water and ethanol under ambient atmosphere. Twice, the product was suspended in methanol (50 mL), sonicated with ultrasound and filtered. The obtained white solid was dried in dynamic vacuum overnight at 110 °C (yield: 8.7g, 63%). ^{1}H NMR (400MHz, DMSO-d^6, 25°C): δ = 4.74 (s, 2 H, CH), 5.61 (s, 2 H, OH), 7.23 (d, $J_{H,H}$ = 8.3 Hz, 4 H, Ph-H), 7.76 (d, $J_{H,H}$ = 8.3 Hz, 4 H, Ph-H), 12.85 (s, 2 H, COOH) ppm. Elemental analysis ($C_{16}H_{14}O_6$·0.2 H_2O): calcd. C 62.83, H 4.75, found C 62.59, H 4.48.

CPO-49-Zn synthesis. In a typical experiment, zinc(II)-nitrate hexahydrate (90 mg, 0.3 mmol) and 4,4'-(1,2-dihydroxyethane-1,2-diyl)dibenzoic acid (30 mg, 0.1 mmol) were placed in a glass vial (Schott, 22 mL). DMF (3 ml) and H_2O (0.05 mL) were added. The mixture was stirred at room temperature until the formation of a clear solution and subsequently placed in a preheated oven at 110 °C for 1 day. The precipitate consisting of colorless crystals was filtered and washed with DMF. Yield: 50 mg, 81% calculated on linker basis for $Zn_2C_{17}H_{11}O_8$·2DMF. Elemental analysis ($Zn_2C_{17}H_{11}O_8$ 1.8 C_3H_7NO 0.35 H_2O): calcd. C 43.97, H 4.00, N 4.12, found C 43.95, H 3.96, N 4.10.

The sample used in the synchrotron experiment was prepared using a slightly different experimental procedure: zinc(II)-nitrate hexahydrate (90 mg, 0.3 mmol) and 4,4'-(1,2-dihydroxyethane-1,2-diyl)dibenzoic acid (90 mg, 0.3 mmol) were placed in a glass vial (Schott, 22 mL). DMF (9 mL) was added. The mixture was stirred at room temperature until the formation of a clear solution and subsequently placed in a preheated oven at 110 °C for 1 day. The colorless precipitate was filtered and washed with DMF.

CPO-49-Mn synthesis. The single crystals measured were obtained using a slightly different experimental procedure: 4,4'-(1,2-dihydroxyethane-1,2-diyl)dibenzoic acid (60 mg, 0.2 mmol) was placed in a glass vial (Schott, 22 mL). DMF (9 mL) was added and the mixture was stirred at room temperature until formation of a clear solution. A solution of manganese(II) acetate tetrahydrate (98 mg, 0.4 mmol) in H_2O (0.9 mL) was added. The formation of a white suspension was observed. The reaction mixture was stirred for 5 minutes before it was placed in a preheated oven at 160 °C for 3 days. Colorless crystals (yield: 10-15mg) and formation of a brown precipitate was observed.

The experimental procedure was subsequently optimized to yield pure bulk samples which also contain single crystals of sufficient size for crystal structure determination: 4,4'-(1,2-dihydroxyethane-1,2-diyl)dibenzoic acid (60 mg, 0.2 mmol) was placed in a glass vial (Schott, 22 mL). DMF (3 mL) was added and the mixture was stirred at room temperature until formation of a clear solution. Formic acid (0.2 mmol) and a solution of manganese(II) acetate tetrahydrate (98 mg, 0.4 mmol) in H_2O (0.3 mL) were added in this order. The formation of a white suspension was observed after addition of manganese(II) acetate solution. The reaction mixture was stirred for 5 minutes. The atmosphere in the reactor was changed to Ar and the reactor was placed in a preheated oven at 160 °C for 3 days. That procedure resulted in higher, but still moderate yield of 40mg and absence of brown impurity (33% yield calculated on linker basis for $Mn_2C_{17}H_{11}O_8 \cdot 2DMF$). Crystals were filtered and washed with DMF. Elemental analysis ($Mn_2C_{17}H_{11}O_8$ 1.95 C_3H_7NO 0.35H_2O): calcd. C 45.59, H 4.24, N 4.54, found C 45.60, H 4.21, N 4.53.

Desolvation of the samples and gas adsorption.

Gas adsorption measurements were carried out on a BELSORP-max instrument. Samples were pre-treated by soaking in chloroform for several times and subsequently heated in a dynamic vacuum at 90 °C overnight. Samples were transferred into the glove-box, where sample cells were filled and transferred to the instrument under inert atmosphere using quick seals. Prior to the sorption experiment, the samples were again heated overnight in a dynamic vacuum at 90 °C.

Thermal analysis

A Netzsch STA 449 F1 Jupiter was used for simultaneous thermogravimetric-differential scanning calorimetry measurements. Measurements were performed in using a flow of pure Ar or O_2/Ar (20/80 mixture) and a heating rate of 2 °C min^{-1}.

Powder X-ray diffraction.

Powder X-ray diffraction was carried out on a Bruker AXS D8 Advance diffractometer equipped with a 9 position multisampler. Data collection was performed using monochromatic Cu $K\alpha_1$ radiation in Bragg-Brentano geometry. A flat sample holder with glass surface was used for the measurements.

Variable temperature powder X-ray diffraction experiments with synchrotron radiation were performed at beamline BM01A of the Swiss-Norwegian Beamlines (SNBL) at ESRF using a custom experimental setup, adapted from literature.[38] The sample was put into a 0.5 mm capillary. Glass fibers were placed on the downstream side of the sample to prevent the sample from being blown out of the capillary. A flow of inert gas was applied through the capillary while the sample was heated with a hot air blower with a rate of 2 °C min^{-1} in the range from room temperature to 200 °C and with the rate 5 °C min^{-1} above 200 °C until the decomposition of the sample. Data was collected using a diffractometer equipped with a Pilatus 2M detector. 2D frames were integrated azimuthal with the *Bubble* tool.[39] Powder X-ray diffraction data and variable temperature powder X-ray diffraction data was analyzed using TOPAS 4.2.[40]

Catalysis

Catalytic reactions were performed in a Biotage microwave vial capped with a septum. In a typical catalytic reaction styrene (0.2 mmol), *tert*-butyl hydroperoxide solution (70 wt.% in H_2O, 0.6 mmol), as-synthesized CPO-49-M (0.01 mmol) and toluene (0.1 mmol) as standard were used. Reaction was run in acetonitrile (1 ml) as a solvent. After addition of the components, the vial was sealed with the septum and placed in a pre-heated bath. The reaction was heated at 60 °C for the specified time period under continuous stirring. Aliquots (50 µL) of the reaction mixture were taken at specified time intervals, diluted in acetonitrile (1 mL) and immediately analyzed using GC-MS. GC-MS analysis was performed with a Shimadzu GCMS-QP2010 Ultra gas chromatograph mass spectrometer equipped with AOC-20i auto sampler and Rxi-5Sil-MS (fused silica, 30.0 m × 0.25 mm × 1.00 µm) column. The following temperature program was used: the temperature was held at 50 °C for 1 min, then raised to 230 °C with a ramp of 9 °C min^{-1}. Injector and interface temperatures were 230 °C. Ion source temperature was 200 °C.

In addition, the catalytic reaction was performed in larger scale by a factor of 3.5. The solid residue from the reaction was used in the N_2 adsorption measurement and supernatant solution for the ICP measurements. The supernatant solution obtained after the centrifugation of catalytic reaction mixture was evaporated in vacuum. The residue obtained in this way was dissolved in 20 mL of 2% nitric acid. This solution was analyzed by inductively coupled plasma optical emission spectrometry (ICP-OES) using an iCAP7600 instrument.

Acknowledgements

We are grateful to Dr. D. Chernyshov, Dr. V. Dyadkin and A. Mikheykin for kind assistance with the measurements at SNBL@ESRF. This research was supported by the Research Council of Norway through grants ISP-KJEMI 209339 and SYNKNOYT 227702 and 247734.

Keywords: Metal-organic frameworks • X-ray diffraction • Adsorption • Heterogeneous catalysis

[1] a) O. M. Yaghi, M. O'Keeffe, N. W. Ockwig, H. K. Chae, M. Eddaoudi, J. Kim, *Nature* **2003**, *423*, 705-714; b) S. Kitagawa, R. Kitaura, S.-i. Noro, *Angew. Chem., Int. Ed.* **2004**, *43*, 2334-2375; c) G. Ferey, *Chem. Soc. Rev.* **2008**, *37*, 191-214.

[2] a) D. Farrusseng, S. Aguado, C. Pinel, *Angew. Chem., Int. Ed.* **2009**, *48*, 7502-7513; b) J. Lee, O. K. Farha, J. Roberts, K. A. Scheidt, S. T. Nguyen, J. T. Hupp, *Chem. Soc. Rev.* **2009**, *38*, 1450-1459; c) J. Liu, L. Chen, H. Cui, J. Zhang, L. Zhang, C.-Y. Su, *Chem. Soc. Rev.* **2014**, *43*, 6011-6061.

[3] Z.-J. Lin, J. Lu, M. Hong, R. Cao, *Chem. Soc. Rev.* **2014**, *43*, 5867-5895.

[4] a) G. Ferey, C. Serre, *Chem. Soc. Rev.* **2009**, *38*, 1380-1399; b) S. Horike, S. Shimomura, S. Kitagawa, *Nat. Chem.* **2009**, *1*, 695-704; c) C. R. Murdock, B. C. Hughes, Z. Lu, D. M. Jenkins, *Coord. Chem. Rev.* **2014**, *258–259*, 119-136; d) A. Schneemann, V. Bon, I. Schwedler, I. Senkovska, S. Kaskel, R. A. Fischer, *Chem. Soc. Rev.* **2014**, *43*, 6062-6096; e) Z. Chang, D.-H. Yang, J. Xu, T.-L. Hu, X.-H. Bu, *Adv. Mater.* **2015**, *27*, 5432-5441.

[5] a) Z. Wang, S. M. Cohen, *Chem. Soc. Rev.* **2009**, *38*, 1315-1329; b) K. K. Tanabe, S. M. Cohen, *Chem. Soc. Rev.* **2011**, *40*, 498-519; c) S. M. Cohen, *Chem. Rev.* **2012**, *112*, 970-1000; d) J. D. Evans, C. J. Sumby, C. J. Doonan, *Chem. Soc. Rev.* **2014**, *43*, 5933-5951; e) Y. Sun, H.-C. Zhou, *Sci. Technol. Adv. Mater.* **2015**, *16*, 054202.

[6] a) S. M. Neville, G. J. Halder, K. W. Chapman, M. B. Duriska, P. D. Southon, J. D. Cashion, J.-F. Létard, B. Moubaraki, K. S. Murray, C. J. Kepert, *J. Am. Chem. Soc.* **2008**, *130*, 2869-2876; b) A. Banisafar, R. L. LaDuca, *Inorg. Chim. Acta* **2011**, *373*, 295-300; c) S. Wang, L. Li, J. Zhang, X. Yuan, C.-Y. Su, *J. Mater. Chem.* **2011**,

21, 7098-7104; d) W. Zhu, C. He, X. Wu, C. Duan, *Inorg. Chem. Commun.* **2014**, *39*, 83-85.

[7] a) R. Kitaura, K. Fujimoto, S.-i. Noro, M. Kondo, S. Kitagawa, *Angew. Chem., Int. Ed.* **2002**, *41*, 133-135; b) X.-Y. Wang, L. Wang, Z.-M. Wang, S. Gao, *J. Am. Chem. Soc.* **2006**, *128*, 674-675; c) K. L. Mulfort, O. K. Farha, C. L. Stern, A. A. Sarjeant, J. T. Hupp, *J. Am. Chem. Soc.* **2009**, *131*, 3866-3868; d) J.-B. Li, X.-Y. Dong, L.-H. Cao, S.-Q. Zang, T. C. W. Mak, *CrystEngComm* **2012**, *14*, 4444-4453; e) Y.-L. Wei, J.-B. Li, W.-C. Song, S.-Q. Zang, *Inorg. Chem. Commun.* **2012**, *15*, 16-20.

[8] a) B. Kesanli, W. B. Lin, *Coord. Chem. Rev.* **2003**, *246*, 305-326; b) L. Q. Ma, C. Abney, W. B. Lin, *Chem. Soc. Rev.* **2009**, *38*, 1248-1256; c) Y. Liu, W. Xuan, Y. Cui, *Adv. Mater.* **2010**, *22*, 4112-4135; d) M. Yoon, R. Srirambalaji, K. Kim, *Chem. Rev.* **2011**, *112*, 1196-1231; e) M. P. Yutkin, D. N. Dybtsev, V. P. Fedin, *Russ. Chem. Rev.* **2011**, *80*, 1009.

[9] a) Y. Ma, A.-L. Cheng, E.-Q. Gao, *Dalton Trans.* **2010**, *39*, 3521-3526; b) Y. Ma, A.-L. Cheng, E.-Q. Gao, *Cryst. Growth Des.* **2010**, *10*, 2832-2834.

[10] a) K. S. Jeong, Y. S. Kim, Y. J. Kim, E. Lee, J. H. Yoon, W. H. Park, Y. W. Park, S.-J. Jeon, Z. H. Kim, J. Kim, N. Jeong, *Angew. Chem., Int. Ed.* **2006**, *45*, 8134-8138; b) S. M. Shin, D. Moon, K. S. Jeong, J. Kim, P. K. Thallapally, N. Jeong, *Chem. Commun.* **2011**, *47*, 9402-9404.

[11] a) H. Furukawa, J. Kim, N. W. Ockwig, M. O'Keeffe, O. M. Yaghi, *J. Am. Chem. Soc.* **2008**, *130*, 11650-11661; b) K. S. Jeong, B. H. Lee, Q. Li, S. B. Choi, J. Kim, N. Jeong, *CrystEngComm* **2011**, *13*, 1277-1279; c) Q. Li, S. M. Shin, D. Moon, K. S. Jeong, N. Jeong, *CrystEngComm* **2013**, *15*, 10161-10164.

[12] A. Clerici, L. Clerici, O. Porta, *Tetrahedron Lett.* **1996**, *37*, 3035-3038.

[13] a) C.-D. Wu, A. Hu, L. Zhang, W. Lin, *J. Am. Chem. Soc.* **2005**, *127*, 8940-8941; b) C.-D. Wu, W. Lin, *Angew. Chem.* **2007**, *119*, 1093-1096; c) T. Gadzikwa, O. K. Farha, K. L. Mulfort, J. T. Hupp, S. T. Nguyen, *Chem. Commun.* **2009**, 3720-3722; d) L. Ma, J. M. Falkowski, C. Abney, W. Lin, *Nat. Chem.* **2010**, *2*, 838-846; e) L. Ma, C.-D. Wu, M. M. Wanderley, W. Lin, *Angew. Chem., Int. Ed.* **2010**, *49*, 8244-8248; f) K. K. Tanabe, C. A. Allen, S. M. Cohen, *Angew. Chem., Int. Ed.* **2010**, *49*, 9730-9733.

[14] A. D. Burrows, K. Cassar, R. M. W. Friend, M. F. Mahon, S. P. Rigby, J. E. Warren, *CrystEngComm* **2005**, *7*, 548-550.

[15] M. Märcz, PhD thesis dissertation, University of Olso **2013**.

[16] a) J. B. DeCoste, G. W. Peterson, *Chem. Rev.* **2014**, *114*, 5695-5727; b) A. Schneemann, S. Henke, I. Schwedler, R. A. Fischer, *ChemPhysChem* **2014**, *15*, 823-839; c) Z. Zhang, Z.-Z. Yao, S. Xiang, B. Chen, *Energy Environ. Sci.* **2014**, *7*, 2868-2899; d) A. Das, D. M. D'Alessandro, *CrystEngComm* **2015**, *17*, 706-718; e) D. Andirova, C. F. Cogswell, Y. Lei, S. Choi, *Microporous Mesoporous Mater.* **2016**, *219*, 276-305; f) B. Li, M. Chrzanowski, Y. Zhang, S. Ma, *Coord. Chem. Rev.* **2016**, *307, Part 2*, 106-129.

[17] A. W. Addison, T. N. Rao, J. Reedijk, J. van Rijn, G. C. Verschoor, *J. Chem. Soc., Dalton Trans.* **1984**, 1349-1356.

[18] a) Q. Ye, X.-S. Wang, H. Zhao, R.-G. Xiong, *Tetrahedron: Asymmetry* **2005**, *16*, 1595-1602; b) S. Chen, J. Zhang, X. Bu, *Inorg. Chem.* **2009**, *48*, 6356-6358; c) Y. Liu, W. Xuan, H. Zhang, Y. Cui, *Inorg. Chem.* **2009**, *48*, 10018-10023; d) J.-W. Sun, J. Zhu, H.-F. Song, G.-M. Li, X. Yao, P.-F. Yan, *Cryst. Growth Des.* **2014**, *14*, 5356-5360.

[19] a) X.-L. Tong, T.-L. Hu, J.-P. Zhao, Y.-K. Wang, H. Zhang, X.-H. Bu, *Chem. Commun.* **2010**, *46*, 8543-8545; b) Q.-Y. Liu, Y.-L. Wang, N. Zhang, Y.-L. Jiang, J.-J. Wei, F. Luo, *Cryst. Growth Des.* **2011**, *11*, 3717-3720; c) X. Tan, J. Zhan, J. Zhang, L. Jiang, M. Pan, C.-Y. Su, *CrystEngComm* **2012**, *14*, 63-66; d) H. Wang, Z. Chang, Y. Li, R.-M. Wen, X.-H. Bu, *Chem. Commun.* **2013**, *49*, 6659-6661.

[20] a) M. Kawano, M. Fujita, *Coord. Chem. Rev.* **2007**, *251*, 2592-2605; b) Y.-Q. Chen, G.-R. Li, Z. Chang, Y.-K. Qu, Y.-H. Zhang, X.-H. Bu, *Chemical Science* **2013**, *4*, 3678-3682; c) J.-P. Zhang, P.-Q. Liao, H.-L. Zhou, R.-B. Lin, X.-M. Chen, *Chem. Soc. Rev.* **2014**, *43*, 5789-5814.

[21] P. D. C. Dietzel, R. E. Johnsen, H. Fjellvag, S. Bordiga, E. Groppo, S. Chavan, R. Blom, *Chem. Commun.* **2008**, 5125-5127.

[22] M. P. Suh, Y. E. Cheon, E. Y. Lee, *Chem. - Eur. J.* **2007**, *13*, 4208-4215.

[23] S. B. Choi, H. Furukawa, H. J. Nam, D.-Y. Jung, Y. H. Jhon, A. Walton, D. Book, M. O'Keeffe, O. M. Yaghi, J. Kim, *Angew. Chem., Int. Ed.* **2012**, *51*, 8791-8795.

[24] L. Wen, P. Cheng, W. Lin, *Chem. Commun.* **2012**, *48*, 2846-2848.

[25] C.-B. Ma, M.-Q. Hu, H. Chen, M. Wang, C.-X. Zhang, C.-N. Chen, Q.-T. Liu, *CrystEngComm* **2010**, *12*, 1467-1473.

[26] a) S. Bourrelly, P. L. Llewellyn, C. Serre, F. Millange, T. Loiseau, G. Férey, *J. Am. Chem. Soc.* **2005**, *127*, 13519-13521; b) H. J. Choi, M. Dincă, J. R. Long, *J. Am. Chem. Soc.* **2008**, *130*, 7848-7850; c) F. Salles, G. Maurin, C. Serre, P. L. Llewellyn, C. Knöfel, H. J. Choi, Y. Filinchuk, L. Oliviero, A. Vimont, J. R. Long, G. Férey, *J. Am. Chem. Soc.* **2010**, *132*, 13782-13788; d) Q. Chen, Z. Chang, W.-C. Song, H. Song, H.-B. Song, T.-L. Hu, X.-H. Bu, *Angew. Chem., Int. Ed.* **2013**, *52*, 11550-11553.

[27] a) S. Takamizawa, E.-i. Nakata, H. Yokoyama, K. Mochizuki, W. Mori, *Angew. Chem.* **2003**, *115*, 4467-4470; b) P. D. C. Dietzel, R. Blom, H. Fjellvag, *Dalton Trans.* **2006**, 586-593; c) C. Serre, S. Bourrelly, A. Vimont, N. A. Ramsahye, G. Maurin, P. L. Llewellyn, M. Daturi, Y. Filinchuk, O. Leynaud, P. Barnes, G. Férey, *Adv. Mater.* **2007**, *19*, 2246-2251; d) P. D. C. Dietzel, R. E. Johnsen, R. Blom, H. Fjellvåg, *Chem. - Eur. J.* **2008**, *14*, 2389-2397; e) R. Matsuda, R. Kitaura, Y. Kubota, T. C. Kobayashi, M. Takata, S. Kitagawa, *Microporous Mesoporous Mater.* **2010**, *129*, 296-303; f) F. Millange, M. I. Medina, N. Guillou, G. Férey, K. M. Golden, R. I. Walton, *Angew. Chem., Int. Ed.* **2010**, *49*, 763-766; g) V. Bon, I. Senkovska, D. Wallacher, A. Heerwig, N. Klein, I. Zizak, R. Feyerherm, E. Dudzik, S. Kaskel, *Microporous Mesoporous Mater.* **2014**, *188*, 190-195; h) V. Bon, I. Senkovska, D. Wallacher, D. M. Többens, I. Zizak, R. Feyerherm, U. Mueller, S. Kaskel, *Inorg. Chem.* **2014**, *53*, 1513-1520; i) H. Sato, W. Kosaka, R. Matsuda, A. Hori, Y. Hijikata, R. V. Belosludov, S. Sakaki, M. Takata, S. Kitagawa, *Science* **2014**, *343*, 167-170; j) V. Bon, J. Pallmann, E. Eisbein, H. C. Hoffmann, I. Senkovska, I. Schwedler, A. Schneemann, S. Henke, D. Wallacher, R. A. Fischer, G. Seifert, E. Brunner, S. Kaskel, *Microporous Mesoporous Mater.* **2015**, *216*, 64-74; k) A. D. Katsenis, A. Puškarić, V. Štrukil, C. Mottillo, P. A. Julien, K. Užarević, M.-H. Pham, T.-O. Do, S. A. J. Kimber, P. Lazić, O. Magdysyuk, R. E. Dinnebier, I. Halasz, T. Friščić, *Nat Commun* **2015**, *6*; l) P. L. Llewellyn, M. Garcia-Rates, L. Gaberová, S. R. Miller, T. Devic, J.-C. Lavalley, S. Bourrelly, E. Bloch, Y. Filinchuk, P. A. Wright, C. Serre, A. Vimont, G. Maurin, *J. Phys. Chem. C* **2015**, *119*, 4208-4216; m) Y. Ma, R. Matsuda, H. Sato, Y. Hijikata, L. Li, S. Kusaka, M. Foo, F. Xue, G. Akiyama, R. Yuan, S. Kitagawa, *J. Am. Chem. Soc.* **2015**, *137*, 15825-15832; n) M. L. Foo, R. Matsuda, Y. Hijikata, R. Krishna, H. Sato, S. Horike, A. Hori, J. Duan, Y. Sato, Y. Kubota, M. Takata, S. Kitagawa, *J. Am. Chem. Soc.* **2016**, *138*, 3022-3030; o) T. Huang, Y.-L. Wang, Q. Yin, B. Karadeniz, H.-F. Li, J. Lu, R. Cao, *CrystEngComm* **2016**, *18*, 2742-2747; p) W. R. Woerner, A. M. Plonka, X. Chen, D. Banerjee, P. K. Thallapally, J. B. Parise, *J. Phys. Chem. C* **2016**, *120*, 360-369.

[28] a) T. Katsuki, K. B. Sharpless, *J. Am. Chem. Soc.* **1980**, *102*, 5974-5976; b) R. Irie, K. Noda, Y. Ito, N. Matsumoto, T. Katsuki, *Tetrahedron Lett.* **1990**, *31*, 7345-7348; c) W. Zhang, J. L. Loebach, S. R. Wilson, E. N. Jacobsen, *J. Am. Chem. Soc.* **1990**, *112*, 2801-2803.

[29] V. Farina, J. T. Reeves, C. H. Senanayake, J. J. Song, *Chem. Rev.* **2006**, *106*, 2734-2793.

[30] H.-F. Yao, Y. Yang, H. Liu, F.-G. Xi, E.-Q. Gao, *J. Mol. Catal. A: Chem.* **2014**, *394*, 57-65.

[31] APEX2, Version 2014.2011-2010; Bruker-AXS: Madison, Wisconsin, USA, 2014.

[32] SAINT, Version 7.68A; Bruker-AXS: Madison, Wisconsin, USA, 2010.

[33] L. Krause, R. Herbst-Irmer, G. M. Sheldrick, D. Stalke, *J. Appl. Crystallogr.* **2015**, *48*, 3-10.

[34] Sheldrick, G. M. XS, Version 2013/2011; Georg-August-Universität Göttingen: Göttingen, Germany, 2013.

[35] G. Sheldrick, *Acta Crystallogr., Sect. A* **2015**, *71*, 3-8.

[36] G. Sheldrick, *Acta Crystallogr., Sect. C* **2015**, *71*, 3-8.

[37] N. A. Jones, S. T. Liddle, C. Wilson, P. L. Arnold, *Organometallics* **2007**, *26*, 755-757.

[38] P. Norby, *J. Am. Chem. Soc.* **1997**, *119*, 5215-5221.

[39] V. Dyadkin, P. Pattison, V. Dmitriev, D. Chernyshov, *J. Synchrotron Radiat.* **2016**, *23*, 825-829.

[40] TOPAS 4.2: General profile and structure analysis software for powder diffraction data, Bruker AXS, Karlsruhe, Germany, 2003.

Entry for the Table of Contents (Please choose one layout)

Layout 1:

FULL PAPER

Two new isostructural metal-organic frameworks based on Zn and Mn and a chiral organic linker were synthesized. Solvent removal leads to single-crystal-to-single-crystal transformation, which proceeds in different fashion for the two metals. The compounds also behave differently upon heating and in catalysis.

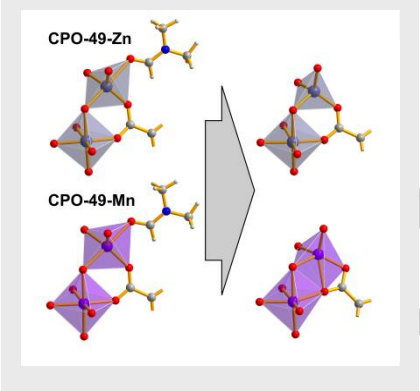

Key Topic*

*Andrey A. Bezrukov, Karl W. Törnroos and Pascal D. C. Dietzel**

Page No. – Page No.

Variation of desolvation behaviour in two isostructural metal-organic frameworks based on a flexible, racemic bifunctional organic linker

*one or two words that highlight the emphasis of the paper or the field of the study